Evaluating and improving the photostability of fluorescent proteins

Nathan C. Shaner*[a], Michael Z. Lin[b], Michael R. McKeown[b], Paul A. Steinbach[b], Kristin L. Hazelwood[c], Michael W. Davidson[c], Roger Y. Tsien[b, d]

[a]Monterey Bay Aquarium Research Institute, 7700 Sandholdt Rd., Moss Landing, CA 95039; [b]Dept. of Pharmacology, University of California, San Diego, 9500 Gilman Dr., San Diego, CA 92093; [c]National High Magnetic Field Laboratory, Florida State University, 1800 E. Paul Dirac Dr., Tallahassee, FL 32310; [d]Dept. of Chemistry and Biochemistry and Howard Hughes Medical Institute, University of California, San Diego, 9500 Gilman Dr., San Diego, CA 92039

ABSTRACT

Fluorescent proteins are the most common and versatile class of genetically encoded optical probes. While structure-guided rational design and directed evolution approaches have largely overcome early problems such as oligomerization, poor folding at physiological temperatures, and availability of wavelengths suitable for multi-color imaging, nearly all fluorescent proteins have yet to be fully optimized. We have developed novel methods for evaluating the current generation of fluorescent proteins and improving their remaining suboptimal properties. Little is yet known about the mechanisms responsible for photobleaching of fluorescent proteins, and inadequate photostability is a chief complaint among end users. In order to compare the performance of fluorescent proteins across the visual spectrum, we have standardized a method used to measure photostability in live cells under both widefield and confocal laser illumination. This method has allowed us to evaluate a large number of commonly used fluorescent proteins, and has uncovered surprisingly complex and unpredictable behaviors in many of these proteins. We have also developed novel methods for selecting explicitly for high photostability during the directed evolution process, leading to the development of highly improved monomeric orange and red fluorescent proteins. These proteins, most notably our photostable derivative of TagRFP, have remarkably high photostability and have proven useful as fusion tags for long-term imaging. Our methods should be applicable to any of the large number of fluorescent proteins still in need of improved photostability.

Keywords: Fluorescent proteins, directed evolution, fluorescence imaging, photostability

1. INTRODUCTION

The field of fluorescent protein science has steadily advanced since the cloning of the first known fluorescent protein from *Aequorea victoria*[1, 2]. Since that time, fluorescent proteins have become some of the most ubiquitously used tools in cell and molecular biology research. While currently existing fluorescent proteins have already proved amenable to a wide variety of applications, several properties of these proteins are not yet optimal, and could stand improvement. Brightness, excitation and emission wavelength, resistance to acidic pH, maturation time, and photostability have been optimized in isolation for many commonly used fluorescent proteins, but no single protein is optimal for all applications. Beyond known fluorescent proteins, researchers have only begun to explore the very large superfamily of fluorescent proteins present in marine invertebrates[3], and many new and useful properties are likely to await discovery. Here, we describe our efforts to engineer wavelength-shifted and optimized variants of the *Discosoma sp.* red fluorescent protein[4] "DsRed," including the development of a novel technique for selecting for bright, highly photostable variants. In addition, we describe a unified characterization of the most commonly used fluorescent proteins, which simplifies the selection process for different applications of these highly diverse tools.

Fluorescent proteins are intrinsically fluorescent polypeptides that form a chromophore autocatalytically through modification of the polypeptide backbone[2, 5-8]. All known fluorescent proteins adopt an 11-stranded β-barrel fold, with a

*nshaner@mbari.org; phone 831-775-2095; fax 831-775-1620

Fluorescence In Vivo Imaging Based on Genetically Engineered Probes: From Living Cells to Whole Body Imaging IV
edited by Alexander P. Savitsky, Yingxiao Wang, Proc. of SPIE Vol. 7191, 719105 · © 2009 SPIE
CCC code: 1605-7422/09/$18 · doi: 10.1117/12.814684

central α-helix which contains the chromophore[1, 3]. In all known wild-type fluorescent proteins, the chromophore is formed by a conserved tripeptide motif (X-Tyr-Gly) by a common three-step mechanism of cyclization, dehydration, and oxidation[1, 3]. Further covalent modifications, as well as interactions with side chains from the surrounding β-barrel, lead to alterations in excitation and emission wavelength as well as other photophysical properties (see **Figure 1**)[1, 3, 5, 7-14].

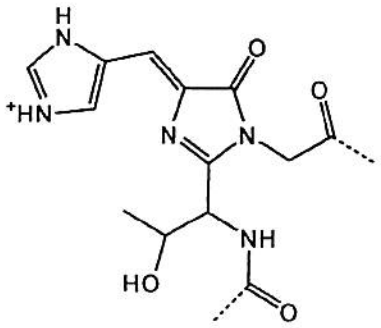

EBFP2 (ex. 383nm, em. 448nm)

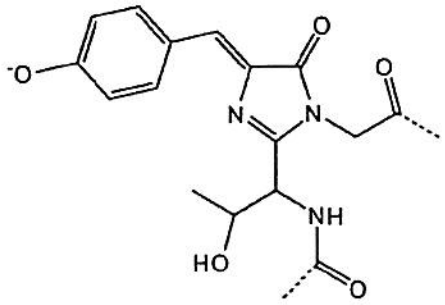

EGFP (ex. 488nm, em. 507nm)

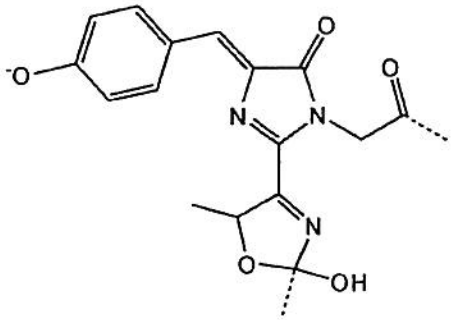

mOrange (ex. 548nm, em. 562nm)

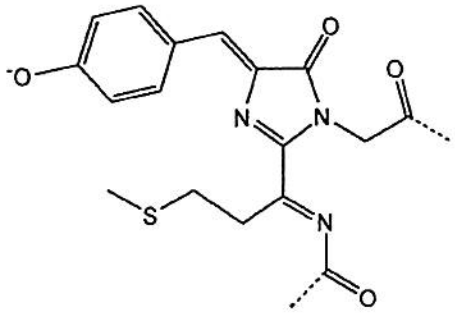

mCherry (ex. 587nm, em. 610nm)

Fig. 1. Representative chromophore structures for four fluorescent protein wavelength classes. Replacement of tyrosine other aromatic residues produces blue (histidine) or cyan (tryptophan) emission; oxidation of the peptide backbone to form an acylimine produces red fluorescence (as for mCherry); further covalent modification of an acylimine-containing chromophore leads to further wavelength shifts, as in mOrange.

The first cloned fluorescent protein was the green fluorescent protein (GFP) isolated from the jellyfish *Aequorea victoria*[2]. While the wild-type protein exhibited poor folding at 37 °C and an undesirable dual-peak excitation spectrum, subsequent mutagenesis and rational design led to vast improvements in its usefulness as an expression marker and fusion tag. *Aequorea* GFP has been engineered into wavelength variants ranging from blue (BFP) and cyan (CFP) to yellow-green (YFP), but proved resistant to red-shifts in emission beyond about 530 nm[2]. While the CFP/YFP pair of fluorescent proteins is used widely for Förster resonance energy transfer (FRET) studies[2, 15, 16], further expansion of available wavelengths was widely desired in the scientific community.

The red fluorescent protein "DsRed," cloned from *Discosoma sp.*[4], partially filled the wavelength gap in available fluorescent proteins. Unfortunately, thorough characterization of DsRed revealed that it had several undesirable properties, including slow maturation, residual green fluorescence, relatively poor solubility, and obligate tetramerization[17]. Because of these shortcomings, wild-type DsRed is of limited utility. Early attempts to improve DsRed resulted in variants with much faster maturation times and improved solubility, but failed to solve the critical issue of tetramerization[18]. Finally, an exhaustive process of directed evolution, requiring a total of 33 mutations relative to wild-type DsRed, led to the development of the first monomeric fluorescent protein, mRFP1[19].

Although mRFP1 proved highly popular and useful, it too had many shortcomings[11]. mRFP1, unlike wild-type DsRed, displays very fast photobleaching, making it unsuitable for time-lapse imaging experiments. Also, mRFP1 displays incomplete maturation, effectively reducing its extinction coefficient. Though mRFP1 is reasonably bright, its quantum yield is much reduced compared to wild-type DsRed. Finally, mRFP1 is highly sensitive to the presence or absence of genetic fusions to its N- or C-terminus, making its successful use in fusion constructs unpredictable. Our efforts to remedy mRFP1's shortcomings and further expand the fluorescent protein color palette led to the development of a set of variants collectively named the "mFruits" which possess a variety of favorable properties for use as genetically encoded reporters[11]. The most popular variant, mCherry, is a direct upgrade from mRFP1, with similar excitation and emission wavelengths but greatly improved photostability and more predictable behavior as a fusion tag.

The successful use of a fluorescent protein (FP) in an imaging experiment can be broken down into several specific requirements. First, the FP should express efficiently and without toxicity in the chosen system, and be bright enough to provide sufficient signal above autofluorescence to be reliably detected and imaged. Second, the FP should exhibit sufficient photostability to be imaged for the duration of the experiment without substantial photobleaching. Third, if the FP is to be expressed as a fusion to another protein of interest, then the FP should not oligomerize and, if monomeric, should not interfere with the localization of its fusion partner. Fourth, the FP should be insensitive to environmental effects that could confound quantitative interpretation of experimental results. Finally, in multiple-labeling experiments, the set of FPs used should give minimal crosstalk in their excitation and emission channels. For more complex imaging experiments, such as those utilizing Förster resonance energy transfer (FRET)[20] or selective optical labeling using photoconvertible FPs[12, 21], additional considerations come into play.

To address the common issue of fast photobleaching, we have developed a new screening method that assays photostability in a medium-throughput format while simultaneously allowing us to monitor the relative brightness of individual clones. This selection scheme allows us to select simultaneously for the most photostable mutants that also maintain an acceptable level of fluorescence emission at the desired wavelength, minimizing the tradeoff of desirable properties that frequently results from single-parameter screens. We applied our photostability screening assay to the directed evolution of variants derived from the bright red monomeric red fluorescent protein TagRFP and the fast-bleaching monomeric orange fluorescent protein mOrange. The resulting variants, TagRFP-T and mOrange2, are 9-fold and 25-fold more photostable than their respective ancestors, and both were found to make excellent fusion partners when expressed in mammalian cells.

2. UNIFORM EVALUATION OF FLUORESCENT PROTEINS

The great variety of fluorescent proteins now available commercially or through academic lab distribution is both a blessing and a curse to end users who must now choose which fluorescent protein is most likely to produce high quality data in a particular experimental application. Commerical claims of superiority do little to help the average researcher make an objective decision, and too frequently critical physical or optical parameters are absent from easily available information on a given fluorescent protein. We sought to remedy this situation by evaluating a large number of commonly used fluorescent proteins, as well as a subset of promising newer fluorescent proteins, to provide a consistent basis for the selection process. Perhaps the most confusing and easily misrepresented property of fluorescent proteins is photostability, which we discuss in more detail below. Other photophysical properties of a number of fluorescent proteins are shown in **Table 1**.

Table 1. Photophysical properties of fluorescent proteins[11, 22-24]

Fluorescent protein	Excitation maximum (nm)	Emission maximum (nm)	Extinction coefficient ($M^{-1} \times cm^{-1}$)	Fluorescence quantum yield	Brightness[a]	pKa	$t_{1/2}$ for maturation at 37°C	$t_{1/2}$ bleach (arc lamp)[b] (s)	$t_{1/2}$ bleach (LSCM)[c] (s)
DsRed[d]	558	583	75,000	0.79	59	4.7	10 h	326	ND[e]
tdTomato[d]	554	581	138,000	0.69	95	4.7	60 min	98	210
mPlum	590	649	41,000	0.10	4.1	< 4.5	100 min	53	ND
mKate	588	635	45,000	0.33	15	6.0	ND	240	ND
mRFP1	584	607	50,000	0.25	13	4.5	< 1 h	8.7	210
mCherry	587	610	72,000	0.22	16	< 4.5	15 min	96	1800
TagRFP[f]	555	584	98,000	0.41	40	3.1	100 min	37	550
TagRFP-T	555	584	81,000	0.41	33	4.6	100 min	337	6900
mApple	568	592	75,000	0.49	37	6.5	30 min	4.8	1300
mOrange	548	562	71,000	0.69	49	6.5	2.5 h	9.0	460
mOrange2	549	565	58,000	0.60	35	6.5	4.5 h	228	2900
mKO	548	559	51,600	0.60	31	5.0	4.5 h	122	930
mCitrine	516	529	77,000	0.76	59	5.7	ND	49	ND
mVenus	515	528	92,200	0.57	53	6.0	ND	15	ND
EGFP/mEGFP	488	507	56,000	0.60	34	6.0	ND	174	5000
mEmerald	487	509	57,500	0.68	39	6.0	ND	169	ND
T-Sapphire	399	511	44,000	0.60	26	4.9	ND	25	ND
mCFP	433/452	475/505	32,500	0.40	13	4.7	ND	64	ND
Cerulean	433/452	475/505	43,000	0.62	27	4.7	ND	36	ND
EBFP	384	450	30,000	0.15	4.5	6.3	ND	0.10	ND
Azurite	377	446	22,000	0.59	13	5.0	ND	19	ND
EBFP2	383	448	32,000	0.56	18	5.3	ND	55	ND

[a] Brightness of fully mature protein, (EC x QY) / 1000

[b] Time (s) to bleach to 50% emission intensity under arc-lamp illumination, at an illumination level that causes each molecule to emit 1000 photons/s initially, as measured in our lab. See below for description of normalization calculations.

[c] Time (s) to bleach to 50% emission intensity measured during laser scanning confocal microscopy, at an average illumination level over the scanned area that causes each molecule to emit an average 1000 photons/s initially, as measured in our lab. A 543nm laser line was used for all proteins except mEGFP, which was bleached with a 488nm laser. See below for detailed description of normalization.

[d] DsRed is an obligate tetramer; tdTomato is a tandem dimer which behaves effectively as a monomer. All other proteins listed on this table are monomeric or very weakly dimeric (for non-monomerized *Aequorea victoria* GFP variants).

[e] ND, not determined.

[f] All measurements were performed in our lab.

2.1 Determination of fluorescent protein photostability with widefield illumination

While most fluorescent proteins in general use have been optimized for brightness and efficiency of expression in mammalian systems, photostability remains a widely varying property which has not been addressed for a number of wavelength classes. Because of this, a standard method for determining the relative photostability of a given fluorescent protein is an essential component of a full characterization scheme. Our technique for measuring photostability provides a reproducible and practical measure under conditions typical for live-cell imaging experiments.

In each bleaching experiment on the microscope using wide-field illumination, we measure the total excitation beam power exiting the microscope objective, with the sample replaced by a micro-integrating sphere attached to an ILC1700

meter (International Light, Newburyport MA), giving a detector current I in amperes. The manufacturer provides a NIST-traceable absolute calibration of this photodetector, $M(\lambda)$, in ampere/watt at 1 nm intervals. We know the relative output of a xenon lamp, $L(\lambda)$, in photons per 1 nm bandwidth, and we have separately measured the transmission of each excitation filter $F(\lambda)$ and dichroic mirror $D(\lambda)$. The energy of each photon of wavelength λ is $hc/\lambda = J(\lambda)$. The number of photons per nm at wavelength $\lambda$is given by $EL(\lambda)F(\lambda)D(\lambda)$, where the overall amplitude factor E is determined by the equation:

$$I = \int EL(\lambda)F(\lambda)D(\lambda)J(\lambda)M(\lambda)d\lambda \quad \cong \quad \sum_{400nm}^{700nm} EL(\lambda)F(\lambda)D(\lambda)J(\lambda)M(\lambda)\Delta\lambda$$

The rate of excitation X of each fluorophore is the integral of the respective contributions from photons of each wavelength interval. Each wavelength interval contributes $EL(\lambda)F(\lambda)D(\lambda)\sigma(\lambda)/A$, where $\sigma(\lambda)$ is the optical cross-section per molecule, and A is the area of illumination. $\sigma(\lambda)$ is proportional to the extinction coefficient $\varepsilon(\lambda)$ as follows: $\sigma(\lambda) = (1000\ cm^3/liter)(\ln 10)\ \varepsilon(\lambda)/(6.023 \times 10^{23}/mole) = (3.82 \times 10^{-21}\ cm^3 \cdot M) \cdot \varepsilon(\lambda)$. Thus:

$$X = \int (E/A)L(\lambda)F(\lambda)D(\lambda)\sigma(\lambda)d\lambda \quad \cong \quad \sum_{400nm}^{700nm} (E/A)L(\lambda)F(\lambda)D(\lambda)\sigma(\lambda)\Delta\lambda$$

The initial rate of emission before any bleaching has occurred is simply XQ, where Q is the fluorescence quantum yield. Meanwhile the camera measures the relative intensity from the microscopic droplet as a function of time, from which the time t_{raw} to drop to 50% of the initial intensity can be readily measured by interpolation. We assume that reciprocity holds for XQ within an order of magnitude of 1000 photons/s, i.e. that bleaching time is inversely proportional to X. This reciprocity assumption has been verified for a few of the fluorescent proteins in **Table 1**, but is expected to break down when X is orders of magnitude greater than 1000 photons/s, i.e. under focused laser illumination. Assuming reciprocity the time to bleach 50% starting from 1000 photons/s emission per chromophore is:

$$t_{1/2} = \frac{t_{raw} XQ}{1000 \text{photons/s}} \tag{1}$$

We must admit that our numerical estimates of photobleaching have undergone some systematic revisions in successive publications, largely due to progressive recognition of the following errors. 1) It is more accurate to perform the above summations over wavelengths rather than to assume monochromaticity, i.e. to use just the meter calibration and extinction coefficient at the center of the excitation passband. 2) The mineral oil in which the microdroplets are suspended must be carefully pre-extracted to remove traces of acidic or quenching contaminants. 3) Many fluorescent proteins refuse to bleach with single exponentials or quantum yields and cannot be quantified as such. 4) Some fluorescent proteins have a very fast phase of partial bleaching that can be missed if one spends too much time focusing and setting up the measurement at too high an intensity. 5) Spatially nonuniform illumination can mean that the calibrated photodiode and the droplets imaged by the camera see different intensities. 6) Many fluorescent proteins display some degree of fluorescence recovery when left in the dark after bleaching.[22]

To address some of these sources of error, we have subsequently reproduced most of our photobleaching measurements using live cells on a number of different microscope setups and have found that while there are small variations in the exact $t_{1/2}$ calculated for each fluorescent protein variant, the rank of photostability among measured fluorescent proteins remains the same in nearly all cases. To address the issue of non-linear bleaching behavior under much stronger illumination intensities, we have also expanded our evaluations to include laser scanning confocal microscopy (LSCM) photobleaching measurements. Representative photobleaching curves for several fluorescent proteins are shown in **Figure 2** below.

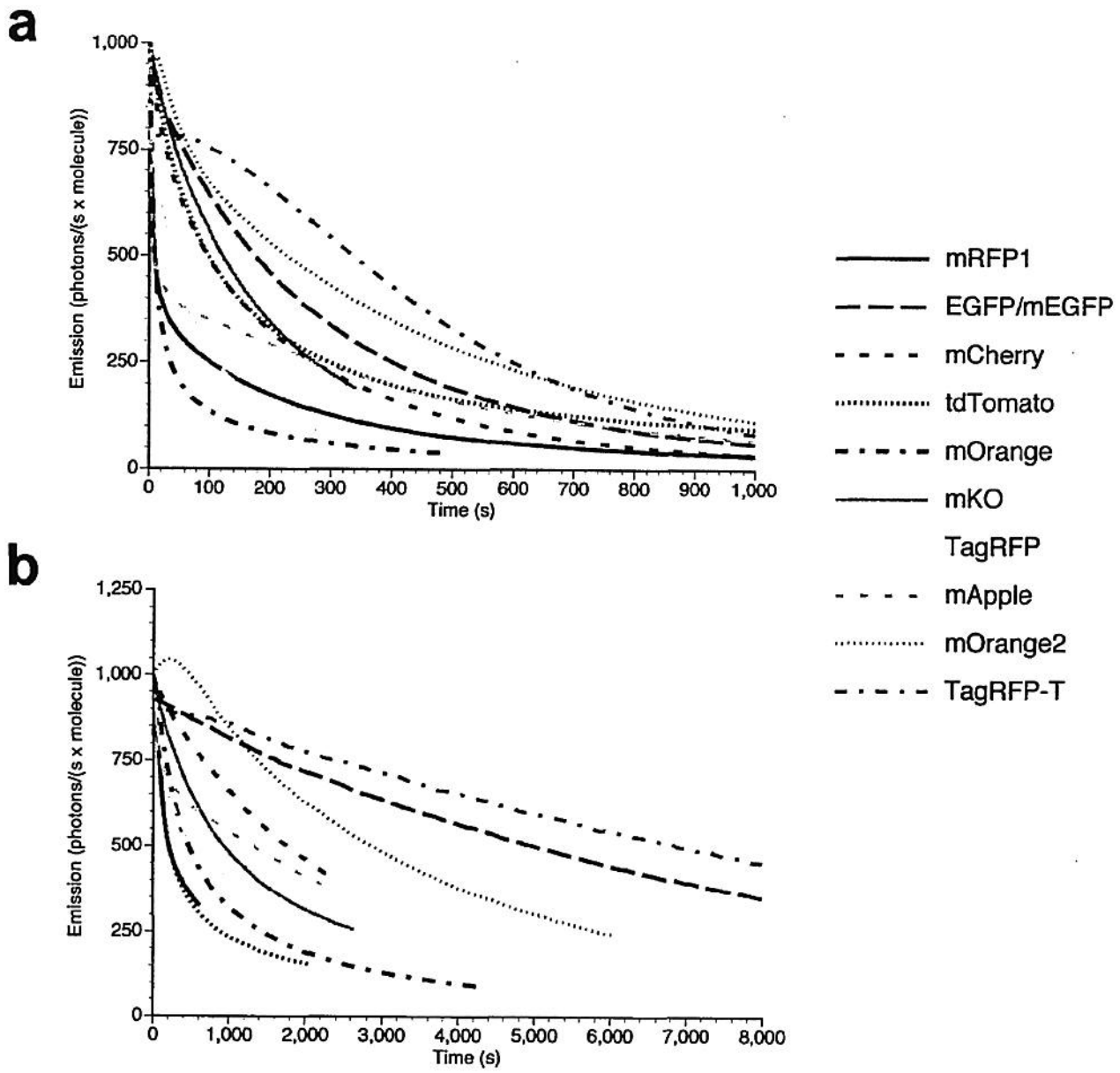

Fig. 2. Photobleaching curves, normalized for initial emission of 1000 photons/s for various fluorescent proteins under (a) widefield and (b) laser scanning confocal illumination.

2.2 Determination of photostability in live cells using laser scanning confocal microscopy

Laser scanning confocal microscopy (LSCM) photobleaching experiments were conducted with N-terminal fusions of the appropriate fluorescent protein to human histone H2B (with a 6-residue linker) to confine fluorescence to the nucleus in order to closely approximate the dimensions of aqueous droplets of purified FPs used in widefield measurements. HeLa-S3 cells (average nucleus diameter = 17μm) were transfected with the H2B construct using Effectene (Qiagen) and maintained in a 5% CO_2 in Delta-T imaging chambers (Bioptechs) for at least 36 hours prior to imaging. The chambers were transferred to a stage adapter (Bioptechs), imaged at low magnification to ensure cell viability, and then photobleaching using a 40x oil immersion objective (Olympus UPlan Apo, NA = 1.00). Laser lines (543 nm, He-Ne and 488 nm, argon-ion) were adjusted to an output power of 50 μW, measured with a FieldMaxII-TO (Coherent) power meter equipped with a high-sensitivity silicon/germanium optical sensor (OP-2Vis, Coherent). The instrument (FV300,

Olympus) was set to a zoom of 4X, a region of interest of 341.2 μm^2 (108 x 108 pixels), a photomultiplier voltage of 650 V, and an offset of 9% with a scan time of 0.181 seconds per frame. Nuclei having approximately the same dimensions and intensity under the fixed instrument settings were chosen for photobleaching assays. Fluorescence using the 543 laser was recorded with a 570 nm dichromatic mirror and 656 nm longpass barrier filter, whereas emission using the 488 laser was directly reflected by a mirror through a 510 nm longpass barrier filter. The photobleaching half-times for LSCM imaging were calculated as the time required to reduce the scan-averaged emission rate to 50% from an initial emission rate of 1000 photons/s per fluorescent protein chromophore. Briefly, the average photon flux (photons/(s x m^2)) over the scanned area of interest was calculated thus:

$$\Phi = \frac{P}{EA} = \frac{P\lambda}{hcA}$$

where P is the output power of the laser measured at the objective in Joules/s, A is the scanned area in m^2, and $E = hc/\lambda$ is the energy of a photon in Joules at the laser wavelength (either 543 nm or 488 nm). The optical cross section (in cm^2) of a fluorescent protein chromophore is given by:

$$\sigma(\lambda) = \frac{(1000 cm^3/L)(\ln 10)\varepsilon(\lambda)}{6.023 \times 10^{23}/mole}$$

where $\varepsilon(\lambda)$ is the extinction coefficient of the fluorescent protein at the laser wavelength in M^{-1} x cm^{-1}. And so the scan-averaged excitation rate per fluorescent molecule is given by:

$$X = \Phi\sigma(\lambda)$$

The time to bleach from an initial scan-averaged rate of 1000 photons/s to 500 photons/s is calculated as in equation (1) above. To produce full bleaching curves, we simply scale the raw time coordinates by the factor $XQ/(1000 photons/s)$ and normalize the intensity coordinate to 1000 photons/s initial emission rate. In most cases, the calculated $t_{1/2}$ for bleaching is more than an order of magnitude greater than that for widefield illumination.

3. A NOVEL SELECTION METHOD FOR PHOTOSTABILITY

Having determined that many commonly used fluorescent proteins display very poor photostability under a number of different assays (see **Table 1**), we developed a novel screening method to select for highly photostable fluorescent protein variants. To photobleach large numbers of bacterial colonies, we utilized a solar simulator (Spectra-Physics 92191-1000 solar simulator with 1600 W mercury arc lamp and two Spectra-Physics SP66239-3767 dichroic mirrors), which produces a collimated beam approximately 10cm in diameter with light intensities of 95 or 141 mW/cm^2 with 525-555 or 548-588 nm bandpass filters (Chroma Technology Corp.) respectively. This intensity, while approximately 100-fold lower than that produced by unattenuated arc lamp illumination and 10^5-fold lower than instantaneous intensities during confocal laser illumination, is sufficient to photobleach the photolabile fluorescent protein mOrange to 50% initial intensity after approximately 10 minutes. This reasonably short time allowed us to quickly screen bacterial libraries of up to 100,000 clones on plates. To minimize heating during illumination, we placed the plates on a custom-built water-cooled aluminum block. At wavelengths necessary to photobleach orange and red fluorescent proteins, we found no substantial decrease in bacterial viability after 2 hours of illumination.

3.1 Selection of a photostable red monomer

We began with the "mFruits" as starting material[11], since these proteins had proven amenable to engineering in the past and their X-ray crystal structures had been solved[14]. To create a better red monomer, we initially undertook a rational design approach, drawing on analysis of mCherry's enhanced photostability and mOrange's higher quantum yield relative to mRFP1. Six generations of directed evolution with constant photostability selection led to the novel variant "mApple," which, though substantially brighter than mCherry, displayed complex photoswitching behavior. This behavior was more pronounced with continuous widefield than with laser-scanning illumination and could be largely eliminated by excitation at alternate wavelengths or by intermittent illumination. However, given our later results using the brighter TagRFP as starting material, we chose not to pursue mApple any further.

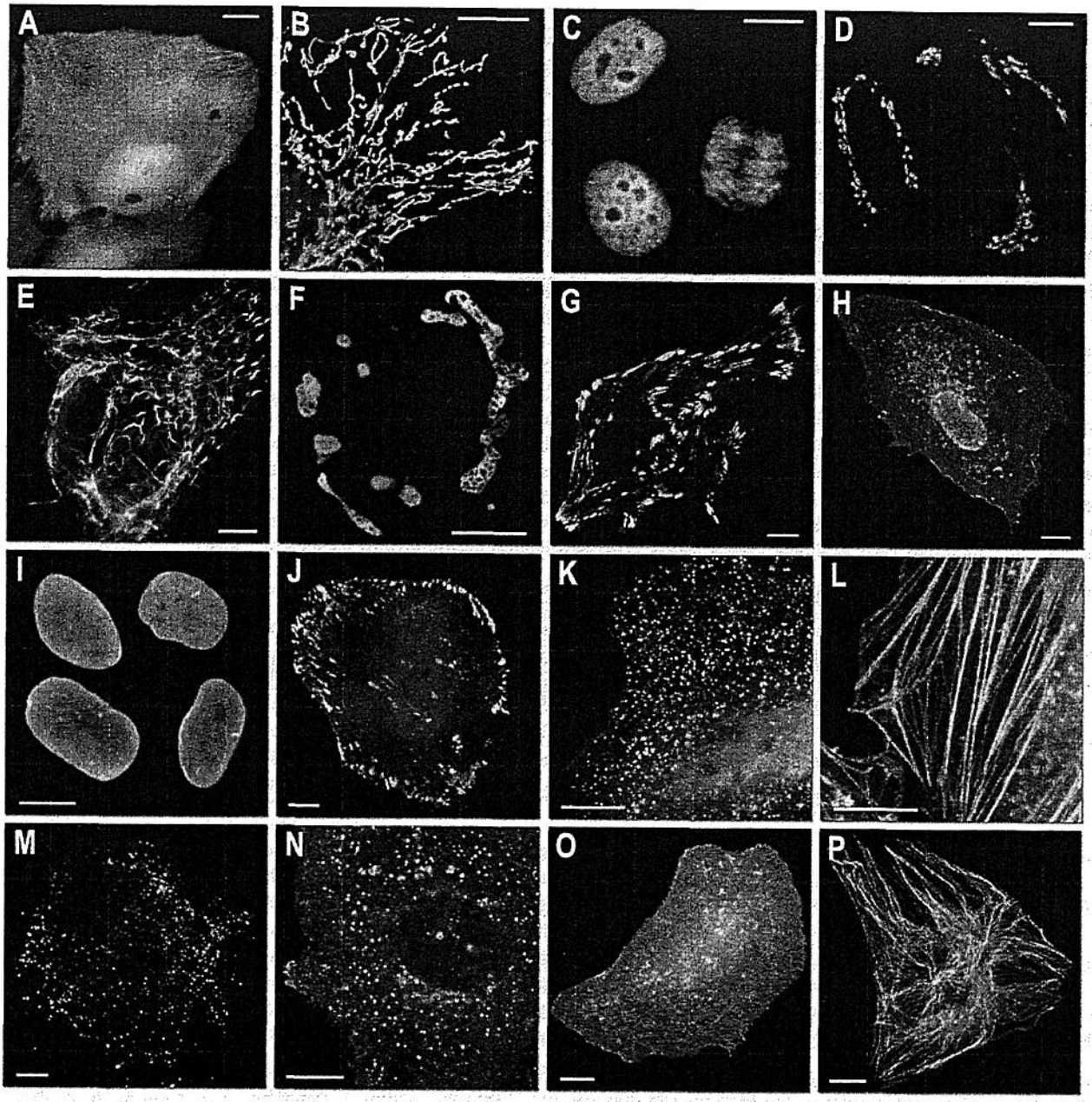

Fig. 3. Fluorescence imaging of TagRFP-T subcellular targeting fusions. N-terminal fusion constructs (linker amino acid length indicated after fusion protein name): (a) TagRFP-T-N1 (N-fusion cloning vector; expression in nucleus and cytoplasm with no specific localization); (b) TagRFP-T-mitochondria-7 (human cytochrome C oxidase subunit VIII); (c) TagRFP-T-H2B-6 (N-terminus; human, showing two interphase nuclei and one nucleus in early anaphase); (d) TagRFP-T-Golgi-7 (N-terminal 81 amino acids of human β-1,4-galactosyltransferase); (e) TagRFP-T-vimentin-7 (human); (f) TagRFP-T-Cx43-7 (rat α-1 connexin-43); (g) TagRFP-T-zyxin-7 (human); C-terminal fusion constructs: (h) TagRFP-T-annexin (A4)-12 (human; illustrated with ionomycin-induced translocation to the plasma and nuclear membranes); (i) TagRFP-T-lamin B1-10 (human); (j) TagRFP-T-vinculin-23 (human); (k) TagRFP-T-clathrin light chain-15 (human); (l) TagRFP-T-β-actin-7 (human); (m) TagRFP-T-peroxisomes-2 (peroximal targeting signal 1; PTS1); (n) TagRFP-T-endosomes-15 (human RhoB GTPase with an N-terminal c-Myc epitope tag); (o) TagRFP-T-farnesyl-5 (20-amino acid farnesylation signal from c-Ha-Ras); (p) TagRFP-T-β-tubulin-6 (human). All TagRFP-T fusion vectors were expressed in HeLa (ATCC; CCL-2) cells. Scale bars are 10 μm.

While the recently developed orange-red monomer TagRFP[25] exhibits remarkable brightness, we have found that its photostability is still far from optimal. In both our standard arc lamp photobleaching and laser scanning confocal assays, we determined that TagRFP bleaches approximately 3-fold faster than mCherry (see **Fig. 2**, and **Table 1**). Thus, we chose this protein as another starting point for improvement of photostability. We first attempted rational design of a mutant library guided by the crystal structure of the closely-related protein eqFP611. With the rationale that chromophore-interacting residues could influence photostability, we performed saturation mutagenesis of Ser158 and Leu199, two residues proximal to the TagRFP chromophore. We then screened this library in bacteria with our solar simulator-based assay, using the 540/30 nm bandpass filter and exposure times of 120 minutes per plate, imaging the plates before and after bleaching to select those colonies that displayed high absolute brightness and a high ratio of post-bleach to pre-bleach fluorescence emission.

From this directed library, we identified one clone, TagRFP S158T (designated "TagRFP-T"), which had a photobleaching half-time of 337 seconds by our standard assay, making it approximately 9-fold more photostable than TagRFP (see **Fig. 2** and **Table 1**). TagRFP-T, which was further modified by appending GFP-like N and C termini, possesses identical excitation and emission wavelength, quantum yield, and maturation time to TagRFP, with only a slightly lower extinction coefficient (81,000 *versus* 98,000 $M^{-1} \times cm^{-1}$) and a higher fluorescence pKa (4.6 *versus* 3.1). We expect that the benefit of increased photostability should offset the small decrease in brightness and increase in acid sensitivity in most applications. Additionally, TagRFP-T matures to apparent completion and has virtually no emission in the green region of the spectrum, making it suitable for co-imaging with green fluorescent proteins. We verified that TagRFP-T remains monomeric by gel filtration (data not shown). Because the S158T mutation is internal, we anticipated that TagRFP-T would perform nearly identically as TagRFP when used as a fusion tag. Indeed, live cell imaging confirmed that TagRFP-T does not interfere with localization of any fusions tested (see **Figure 3**).

3.2 Selection of a photostable orange monomer

We next attempted to engineer a photostable variant of mOrange[11], which is the brightest of the previously engineered mRFP1 variants, but exhibits relatively fast bleaching. As with most fluorescent protein optimization efforts, we used iterative random and directed mutagenesis with selection using the solar simulator. Initially, a randomly mutagenized library of mOrange was screened by photobleaching with 525-555 nm for 15 to 20 minutes per plate (a time sufficient to bleach mOrange to ~25% of its initial brightness) and selecting the brightest post-bleach clones by eye. This screen identified a single clone, mOrange F99Y, which had approximately two-fold improved photostability. Saturation mutagenesis of residue 99 and residues 97 and 163, which we imagined could have synergistic interactions with residue 99, did not yield further improvements.

We then constructed a randomly mutagenized library of mOrange F99Y, and screened with a longer illumination time of 40 minutes per plate. This round of screening identified the additional mutation Q64H, which conferred a remarkable ~10-fold increase in photostability over the F99Y single mutant. Again, saturation mutagenesis of residues 64 and 99 along with surrounding residues 97 and 163 failed to produce clones that were improved over the original clone identified in the random screen. Additionally, we found that the Q64H mutation alone did not confer substantially enhanced photostability, but rather required the presence of the F99Y mutation (data not shown). Two further rounds of directed evolution with continued selection for photostability (540/30 nm filter, 40 minutes per plate) improved the folding efficiency with mutations E160K and G196D, giving the final clone, "mOrange2."

The highly desirable increase in photostability achieved in mOrange2 is balanced by a modest decrease in quantum yield (0.60 versus 0.69) and extinction coefficient (58,000 versus 72,000 $M^{-1} \times c\ m^{-1}$), together corresponding to a 30% decrease in brightness compared to mOrange. It also exhibits slightly shifted excitation and emission peaks (549nm and 565nm) and an increased maturation half-time (4.5 hours versus 2.5 hours). However, its photostability under arc lamp illumination is over 25-fold greater than that of mOrange (**Fig. 2**), making it nearly twice as photostable as mKO[9], the previously most photostable known orange monomer[24], approximately 6-fold more photostable than TagRFP[25], and about 1.3-fold more photostable than EGFP[24] (see **Table 1**). During laser scanning confocal imaging, mOrange2 is approximately 6-fold more photostable than mOrange and 3-fold more photostable than mKO (see **Fig. 2b**). Curiously, the brightness and maturation time of mOrange2 are quite similar to those for mKO. mOrange2 remains acid-sensitive with a pKa of 6.5, making it undesirable for targeting to acidic compartments, but attractive as a possible marker for exocytosis or other pH-variable processes[26]. Also, because it still contains a small fraction of immature (but non-fluorescent) chromophore, mOrange2 may not be an ideal FRET acceptor. As with TagRFP-T, we verified that mOrange2 remained monomeric using gel filtration. Like TagRFP-T, mOrange2 is well behaved when used as a fusion partner for all proteins tested.

4. FUTURE DIRECTIONS

While we have found many novel properties through stepwise engineering of mRFP1 variants, it is reasonable to assume that fluorescent proteins are capable of even more complex and useful photophysical behaviors. Future experiments should focus on exploring the limits of wavelength shift, especially in the far-red, and the engineering of controllable, efficient, and reversible photoactivatable proteins. Further optimization of photostability should be possible through applications of our solar simulator technique as well as the continued development of novel selection methods. Elucidation of the primary mechanisms for photobleaching and photoactivation through mass spectrometry and X-ray crystallography will provide starting points for rational design of these properties. Development of a high-efficiency and easily adaptable orange-red FRET pair is also a priority, as it will open up additional possibilities for live-cell imaging of biochemical processes. Finally, continued exploration of the diversity of wild-type fluorescent proteins will likely lead to the discovery of novel properties already evolved by nature.

5. ACKNOWLEDGEMENTS AND AUTHOR CONTRIBUTIONS

L. A. Gross performed mass spectroscopy. S. R. Adams performed gel filtration experiments. We thank R. E. Campbell and C. T. Dooley for helpful discussion. Sequencing services were provided by the University of California, San Diego Cancer Center shared sequencing resource and the Florida State University Bioanalytical and Molecular Cloning DNA Sequencing Laboratory. N.C.S. was a Howard Hughes Medical Institute Predoctoral fellow during this work. This work was additionally supported by NIH (NS27177 and GM72033) and the Howard Hughes Medical Institute.

N.C.S. designed the photostability selection protocol, performed all directed evolution and physical characterization of mApple and mOrange2, analyzed and organized all data collected by other authors, and prepared the manuscript; M.Z.L. and M.R.M. performed directed evolution and physical characterization of TagRFP-T; P.A.S. designed the home-built components of the solar simulator apparatus and performed photobleaching measurements of purified proteins; K.L.H. and M.W.D. constructed mammalian expression vectors and performed all microscopy experiments involving live cells.

Sequences for mOrange2, mApple, and TagRFP-T have been deposited under accession numbers DQ336159, DQ336160, and EU582019, respectively.

REFERENCES

[1] Prasher, D.C., Eckenrode, V.K., Ward, W.W., Prendergast, F.G. & Cormier, M.J., "Primary structure of the Aequorea victoria green-fluorescent protein," Gene 111, 229-233 (1992).

[2] Tsien, R.Y., "The green fluorescent protein," Annu Rev Biochem 67, 509-544 (1998).

[3] Shagin, D.A. et al., "GFP-like proteins as ubiquitous metazoan superfamily: evolution of functional features and structural complexity," Mol Biol Evol 21, 841-850 (2004).

[4] Matz, M.V. et al., "Fluorescent proteins from nonbioluminescent Anthozoa species," Nat Biotechnol 17, 969-973 (1999).

[5] Gross, L.A., Baird, G.S., Hoffman, R.C., Baldridge, K.K. & Tsien, R.Y., "The structure of the chromophore within DsRed, a red fluorescent protein from coral," Proc Natl Acad Sci U S A 97, 11990-11995 (2000).

[6] Petersen, J. et al., "The 2.0-A crystal structure of eqFP611, a far red fluorescent protein from the sea anemone Entacmaea quadricolor," J Biol Chem 278, 44626-44631 (2003).

[7] Remington, S.J. et al., "zFP538, a yellow-fluorescent protein from Zoanthus, contains a novel three-ring chromophore," Biochemistry 44, 202-212 (2005).

[8] Yarbrough, D., Wachter, R.M., Kallio, K., Matz, M.V. & Remington, S.J., "Refined crystal structure of DsRed, a red fluorescent protein from coral, at 2.0-A resolution," Proc Natl Acad Sci U S A 98, 462-467 (2001).

[9] Karasawa, S., Araki, T., Nagai, T., Mizuno, H. & Miyawaki, A., "Cyan-emitting and orange-emitting fluorescent proteins as a donor/acceptor pair for fluorescence resonance energy transfer," Biochem J 381, 307-312 (2004).

[10] Mizuno, H. et al., "Photo-induced peptide cleavage in the green-to-red conversion of a fluorescent protein," Mol Cell 12, 1051-1058 (2003).
[11] Shaner, N.C. et al., "Improved monomeric red, orange and yellow fluorescent proteins derived from Discosoma sp. red fluorescent protein," Nat Biotechnol 22, 1567-1572 (2004).
[12] Wiedenmann, J. et al., "EosFP, a fluorescent marker protein with UV-inducible green-to-red fluorescence conversion," Proc Natl Acad Sci U S A 101, 15905-15910 (2004).
[13] Wilmann, P.G., Petersen, J., Devenish, R.J., Prescott, M. & Rossjohn, J., "Variations on the GFP chromophore: A polypeptide fragmentation within the chromophore revealed in the 2.1-A crystal structure of a nonfluorescent chromoprotein from Anemonia sulcata," J Biol Chem 280, 2401-2404 (2005).
[14] Shu, X., Shaner, N.C., Yarbrough, C.A., Tsien, R.Y. & Remington, S.J., "Novel chromophores and buried charges control color in mFruits," Biochemistry 45, 9639-9647 (2006).
[15] Nguyen, A.W. & Daugherty, P.S., "Evolutionary optimization of fluorescent proteins for intracellular FRET," Nat Biotechnol 23, 355-360 (2005).
[16] Rizzo, M.A., Springer, G.H., Granada, B. & Piston, D.W., "An improved cyan fluorescent protein variant useful for FRET," Nat Biotechnol 22, 445-449 (2004).
[17] Baird, G.S., Zacharias, D.A. & Tsien, R.Y., "Biochemistry, mutagenesis, and oligomerization of DsRed, a red fluorescent protein from coral," Proc Natl Acad Sci U S A 97, 11984-11989 (2000).
[18] Bevis, B.J. & Glick, B.S., "Rapidly maturing variants of the Discosoma red fluorescent protein (DsRed)," Nat Biotechnol 20, 83-87 (2002).
[19] Campbell, R.E. et al., "A monomeric red fluorescent protein," Proc Natl Acad Sci U S A 99, 7877-7882 (2002).
[20] Zhang, J., Campbell, R.E., Ting, A.Y. & Tsien, R.Y., "Creating new fluorescent probes for cell biology," Nat Rev Mol Cell Biol 3, 906-918 (2002).
[21] Patterson, G.H. & Lippincott-Schwartz, J., "Selective photolabeling of proteins using photoactivatable GFP," Methods 32, 445-450 (2004).
[22] Shaner, N.C. et al., "Improving the photostability of bright monomeric orange and red fluorescent proteins," Nat Methods 5, 545-551 (2008).
[23] Shaner, N.C., Patterson, G.H. & Davidson, M.W., "Advances in fluorescent protein technology," J Cell Sci 120, 4247-4260 (2007).
[24] Shaner, N.C., Steinbach, P.A. & Tsien, R.Y., "A guide to choosing fluorescent proteins," Nat Methods 2, 905-909 (2005).
[25] Merzlyak, E.M. et al., "Bright monomeric red fluorescent protein with an extended fluorescence lifetime," Nat Methods 4, 555-557 (2007).
[26] Miesenbock, G., De Angelis, D.A. & Rothman, J.E., "Visualizing secretion and synaptic transmission with pH-sensitive green fluorescent proteins," Nature 394, 192-195 (1998).